Journal of Architectural Environment & Structural Engineering Research

https://ojs.bilpublishing.com/index.php/jaeser

ARTICLE

Failure Evaluation of Reinforced Concrete Beams Using Damage Mechanics and Classical Laminate Theory

José Mário Feitosa Lima **Geraldo José Belmonte dos Santos** **Paulo Roberto Lopes Lima***

State University of Feira de Santana, Technology Department, Feira de Santana, Bahia, 44030-900, Brazil

ARTICLE INFO

Article history

Received: 30 August 2022

Revised: 16 September 2022

Accepted: 20 October 2022

Published Online: 26 October 2022

Keywords:

Reinforced concrete

Damage mechanics

Finite element method

Laminate theory

ABSTRACT

The prediction of the behavior of reinforced concrete beams under bending is essential for the perfect design of these elements. Usually, the classical models do not incorporate the physical nonlinear behavior of concrete under tension and compression, which can underestimate the deformations in the structural element under short and long-term loads. In the present work, a variational formulation based on the Finite Element Method is presented to predict the flexural behavior of reinforced concrete beams. The physical nonlinearity due cracking of concrete is considered by utilization of damage concept in the definition of constitutive models, and the lamination theory it is used in discretization of section cross of beams. In the layered approach, the reinforced concrete element is formulated as a laminated composite that consists of thin layers, of concrete or steel that has been modeled as elastic-perfectly plastic material. The comparison of numerical load-displacement results with experimental results found in the literature demonstrates a good approximation of the model and validates the application of the damage model in the Classical Laminate Theory to predict mechanical failure of reinforced concrete beam. The results obtained by the numerical model indicated a variation in the stress–strain behavior of each beam, while for under-reinforced beams, the compressive stresses did not reach the peak stress but the stress–strain behavior was observed in the nonlinear regime at failure, for the other beams, the concrete had reached its ultimate strain, and the beam's neutral axis was close to the centroid of the cross-section.

1. Introduction

The nonlinear numerical analysis of reinforced concrete structures has been implemented to predict both the reduction in stiffness with the increase in deformations, as well as the mechanism and process of failure [1]. The incorporation of nonlinear stress–strain models under tension and/or compression [2-4] has changed the constitutive equations of concrete.

Concrete is a cement-based composite material whose

*Corresponding Author:
Paulo Roberto Lopes Lima,
State University of Feira de Santana, Technology Department, Feira de Santana, Bahia, 44030-900, Brazil;
Email: lima.prl@pq.cnpq.br

DOI: https://doi.org/10.30564/jaeser.v5i4.5028

mechanical properties depend on the constituents and interfaces between them. Its behavior is defined by the pre-existence of pores, voids, inclusions, and microcracks prior to loading, which induces: (i) a post-cracking behavior of strain softening; (ii) progressive deterioration of the mechanical properties; (iii) volumetric expansion; (iv) induced anisotropy; (v) asymmetry in response to traction and compression; (iv) considered fragile in traction and quasi-ductile in compression. In contrast, reinforced concrete uses steel reinforcements embedded in the cementitious matrix to increase the strength and stiffness of the composite, primarily in the tension regions. Reinforced concrete exhibits an initially linear elastic behavior with a progressive increase in loading that progress to a nonlinear inelastic behavior induced by crack propagation and concrete crushing or steel yielding. Mathematical modeling of the nonlinear inelastic behavior of concrete, without considering creep, is typically based on plasticity theory, continuous damage theory, fracture mechanics, or a combination of these [5-12].

The isotropic Mazar damage model [13] allows the continuous representation of the structural model even after concrete cracking has generated good results in the modeling of reinforced concrete structures [14,15]. This model uses theories based on the mechanics of continuous damage that define the constitutive laws of concrete. Only one internal variable is required to apply this model and its evolution law is easily obtained by performing tensile and compression tests on the material.

In terms of discrete representation of reinforced concrete structures, the most common model for numerical analysis has been the use of the finite element method, wherein the concrete and reinforcement bars are modeled separately using two different types of elements. An additional approach has been used with the adoption of lamination, wherein the structural element is divided into several layers [2,16]. Based on the classical laminate theory, this model associates a specific type of material with each layer of the beam and considers the perfect adhesion between the layers. By monitoring the stresses and strains in each layer, the commencement of cracking in the concrete and the yielding of the reinforcement can be identified, thus resulting in a more realistic evaluation of the behavior of the structural elements of reinforced concrete.

The objective of this study is to assess the effectiveness of damage mechanics and classical lamination theory in the failure prediction of reinforced concrete beams. For this purpose, a variational formulation model was developed based on such theories and the principle of virtual work. Subsequently, it was applied using the finite element method (FEM) and the obtained results were compared with the experimental results reported in the literature.

2. Problem Formulation and Numerical Modeling

2.1 Materials Modelling

The model proposed by Mazars [13] is based on experimental evidence observed in the behavior of concrete under uniaxial tension and compression, wherein the material degrades owing to distributed microcracking caused by tensile stresses. In this model, the damage is represented by scalar variable D, whose evolution occurs only when an equivalent strain measure, $\tilde{\varepsilon}$, exceeds a threshold value, ε_{d0}, corresponding to the tensile strength of the concrete. The equivalent strain $\tilde{\varepsilon}$ represents the elongation local state and is given by:

$$\tilde{\varepsilon} = \sqrt{<\varepsilon_1>_+^2 + <\varepsilon_2>_+^2 + <\varepsilon_3>_+^2} \tag{1}$$

where $<\varepsilon_i>_+$ is the positive part of the elongation in the principal direction i and is defined as

$$<\varepsilon_i>_+ = \frac{1}{2}(\varepsilon_i + |\varepsilon_i|) = \begin{cases} \varepsilon_i, if\ \varepsilon_i > 0 \\ 0, if\ \varepsilon_i \le 0 \end{cases} \tag{2}$$

In the pre-cracking phase ($\varepsilon \le \varepsilon_{d0}$), the concrete exhibits its linear elastic behavior. Whereas in the post-cracking phase, when the strain is greater than the elastic strain limit ($\varepsilon > \varepsilon_{d0}$), the concrete exhibits nonlinear elastic behavior when the initial elastic modulus E_0 is progressively damaged.

Thus, the uniaxial stress–strain behavior of concrete can be established by:

$$\sigma = \begin{cases} E_o\, \varepsilon, & \varepsilon \le \varepsilon_{d0} \\ (1-D)\, E_o \varepsilon, & \varepsilon > \varepsilon_{d0} \end{cases} \tag{3}$$

In Equation (3), the damage parameter D varies between 0 (when $\varepsilon \le \varepsilon_{d0}$) and 1 (when the material is completely damaged), as expressed by (see [14,15]):

$$D = \alpha_T D_T + \alpha_C D_C \tag{4}$$

with

$$\alpha_T = \frac{\sum_i <\varepsilon_{T_i}>_+}{\sum_i <\varepsilon_{T_i}>_+ + \sum_i <\varepsilon_{C_i}>_+} \tag{5}$$

$$\alpha_C = \frac{\sum_i <\varepsilon_{C_i}>_+}{\sum_i <\varepsilon_{T_i}>_+ + \sum_i <\varepsilon_{C_i}>_+} \tag{6}$$

$$D_T(\tilde{\varepsilon}) = 1 - \frac{\varepsilon_{d0}(1-A_T)}{\tilde{\varepsilon}} - \frac{A_T}{\exp\left[B_T(\tilde{\varepsilon}-\varepsilon_{d0})\right]}, \text{ and} \tag{7}$$

$$D_C(\tilde{\varepsilon}) = 1 - \frac{\varepsilon_{d0}(1-A_C)}{\tilde{\varepsilon}} - \frac{A_C}{exp\left[B_C(\tilde{\varepsilon}-\varepsilon_{d0})\right]} \tag{8}$$

where $\alpha_T + \alpha_C = 1$, ε_{T_i} and ε_{C_i} are the components of the principal strains determined by the positive and negative parts, respectively. The values A_T, B_T, A_C, B_C and ε_{d0} are the experimental parameters obtained from the material tests.

For the reinforcing steel bars, the linear elastic behavior between the stress and strain before yield deformation is assumed to be $\sigma_s = E_s\varepsilon, if\, \varepsilon < \varepsilon_y$, where E_s is the elastic modulus of the steel. After yielding $\varepsilon \geq \varepsilon_y$, the stress is assumed to be constant, $\sigma_s = f_y$, where f_y is the yielding stress of the steel and exhibits linearly elastic–perfectly plastic behavior.

In this study, the cross section of the beams was discretized in NC layers of thickness h_k (k=1,..., NC), as shown in Figure 1.

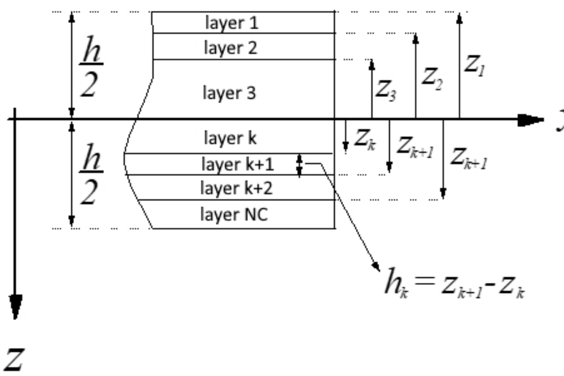

Figure 1. Discretization of the laminated beam

Classical laminate theory establishes that the laminae that form the laminate are in a plane stress state. In this context, and based on the generalized Hooke's law for homogeneous and isotropic materials, the following relationship between stresses and strains in each layer of the laminate is valid [16].

$$\begin{Bmatrix} \sigma_x \\ \sigma_y \\ \tau_{xy} \end{Bmatrix} = \begin{bmatrix} Q_{11}^{(k)} & Q_{12}^{(k)} & 0 \\ Q_{12}^{(k)} & Q_{22}^{(k)} & 0 \\ 0 & 0 & Q_{66}^{(k)} \end{bmatrix} \begin{Bmatrix} \varepsilon_x \\ \varepsilon_y \\ \gamma_{xy} \end{Bmatrix} \tag{9}$$

where the quantities $Q_{11}^{(k)}$, $Q_{12}^{(k)}$, $Q_{22}^{(k)}$ and $Q_{66}^{(k)}$ are the mechanical constants related to the engineering properties of the layer material, as defined below.

$$Q_{11}^{(k)} = Q_{22}^{(k)} = \left(\frac{E}{1-\nu^2}\right)^{(k)} \tag{10}$$

$$Q_{12}^{(k)} = \left(\frac{\nu E}{1-\nu^2}\right)^{(k)}, \text{ and} \tag{11}$$

$$Q_{66}^{(k)} = \left(\frac{E}{2(1+\nu)}\right)^{(k)} = (G)^{(k)} \tag{12}$$

where E and G represent the longitudinal and transverse moduli of elasticity of the material, respectively, which make up the layer of the laminate; and ν is Poisson's ratio.

In the formulation proposed here, the elastic modulus present in quantities $Q_{11}^{(k)}$, $Q_{12}^{(k)}$, $Q_{22}^{(k)}$ and $Q_{66}^{(k)}$ incorporates the damage that occurs in the concrete layers and is given by Equations (4)–(8). When the layer is steel, the stress–strain relationship incorporates plastic strain after the yield limit.

The classical laminate theory is typically developed only for laminates formed by orthotopic or isotropic materials [16]. However, this theory can be considered as an extension of the classical theory to address problems involving materials subject to damage and plasticity.

2.2 Internal Stress Resultants in the Laminated Section

The model used in the study, which appears in the Euler–Bernoulli Beam theory in a single stress component σ_x in Equation (9) used for the analysis of beams, is believed to have only one non-zero strain component ε_x, as given below.

$$\sigma_x = Q_{11}^{(k)} \varepsilon_x \tag{13}$$

The internal stresses in the generic cross-section of the laminate of area *A* are related by the following equations.

$$N = \int_A \sigma_x \, dA = b \int_{-h/2}^{h/2} \sigma_x dz \tag{14}$$

$$M = \int_A \sigma_x \, z dA = b \int_{-h/2}^{h/2} \sigma_x z dA \tag{15}$$

where *N* denotes the normal force; *M* denotes the bending moment; *b* denotes the width of the section; and *h* denotes its height.

For a laminated cross section, as shown in Figure 1, the evaluation of these internal stress resultants is performed by adding the contribution from each lamina; in this process, different materials are considered. With the development of the addition, we obtain Equations (16) and (17), which are compact expressions of the resultants.

$$N = A_{11}\frac{\partial u_0}{\partial x} - B_{11}\frac{\partial^2 w_0}{\partial x^2} \tag{16}$$

$$M = B_{11}\frac{\partial u_0}{\partial x} - D_{11}\frac{\partial^2 w_0}{\partial x^2} \tag{17}$$

where

$$A_{11} = b\sum_{k=1}^{NC} Q_{11}^{(k)}(z_{k+1} - z_k) \tag{18}$$

$$B_{11} = \frac{b}{2}\sum_{k=1}^{NC} Q_{11}^{(k)}\left(z_{k+1}^2 - z_k^2\right) \tag{19}$$

$$D_{11} = \frac{b}{3}\sum_{k=1}^{NC} Q_{11}^{(k)}\left(z_{k+1}^3 - z_k^3\right) \tag{20}$$

The quantities A_{11}, B_{11}, and D_{11} are associated with the term [1, 1] of the matrices of extensional stiffness [A], bending stiffness [B], and coupling [D], respectively, as they are referred to in the classical laminate theory [16]. However, note that Equations (18)–(20) incorporate the width of section *b* of the beam, which is not present in the equations of classical laminate theory.

2.3 Principle of Virtual Works

In this study, FEM was used to model the laminated beam, and the principle of virtual work was used to write equilibrium equations and transform the continuous problem into a discrete problem.

Given that the structural system will be in equilibrium, if the total virtual work of the applied forces is zero, for any compatible virtual (and infinitesimal) displacement, the initial problem is determining the virtual work done by the internal forces and the virtual work done by external forces.

The virtual work done by the internal forces for the problem is given by:

$$\delta W_{int} = \int_V \sigma_x \delta\varepsilon_x dV \tag{21}$$

where $\delta\varepsilon_x$ is the variation in the strain component ε_x; and V is the volume of the beam.

For the laminated section shown in Figure 1, we obtain the following.

$$\delta W_{int} = \int_0^L \left[\left(A_{11}\frac{\partial u_0}{\partial x} - B_{11}\frac{\partial^2 w_0}{\partial x^2}\right)\delta\left(\frac{\partial u_0}{\partial x}\right) - \left(B_{11}\frac{\partial u_0}{\partial x} - D_{11}\frac{\partial^2 w_0}{\partial x^2}\right)\delta\left(\frac{\partial^2 w_0}{\partial x^2}\right)\right] dx \tag{22}$$

The virtual work done by the external forces, assuming that the loads are applied directly to the axis of the structure to produce bending, is given by:

$$\delta W_{ext} = \int_0^L [p(x)\delta u_0 + q(x)\delta w_0]\, dx + \left[\bar{F}_x \delta u_0 + \bar{F}_z \delta w_0 - \bar{M}\delta\left(\frac{\partial w_0}{\partial x}\right)\right]_0^L \tag{23}$$

where $p(x)$ and $q(x)$ represent the distributed loads of the domain according to the axial x axis and transverse z axis, respectively; $\bar{F}_x$ and $\bar{F}_z$ represent the forces applied at the beam ends ($x = 0$ and $x = L$), respectively; and $\bar{M}$ represents the external moments applied at the same ends.

By applying the equilibrium condition imposed by the principle of virtual work (PTV), that is, $\delta W_{int} = \delta W_{ext}$, the differential equations of the problem can be instituted, previously making the variations of displacements in the domain portions in Equations (22) and (23) through integration by parts.

This result in the system of differential equations associated with the model:

$$A_{11}\frac{\partial^2 u_0}{\partial x^2} - B_{11}\frac{\partial^3 w_0}{\partial x^3} = -p(x) \quad \text{or} \quad \frac{\partial N}{\partial x} = -p(x) \tag{24}$$

$$B_{11}\frac{\partial^3 u_0}{\partial x^3} - D_{11}\frac{\partial^4 w_0}{\partial x^4} = q(x) \quad \text{or} \quad \frac{\partial^2 M}{\partial x^2} = q(x) \tag{25}$$

Because of the application of PTV, the following boundary conditions are extracted at $x = 0$ and $x = L$, inherent to the model:

$$u_0 = \bar{u}_0 \text{ and } \delta u_0 = \delta\bar{u}_0 \quad \text{or} \quad N = \bar{F}_x \tag{26}$$

$$w_0 = \bar{w}_0 \text{ and } \delta w_0 = \delta\bar{w}_0 \quad \text{or} \quad Q = \bar{F}_z \tag{27}$$

$$\frac{\partial w_0}{\partial x} = \frac{\partial \bar{w}_0}{\partial x} \text{ and } \delta\left(\frac{\partial w_0}{\partial x}\right) = \delta\left(\frac{\partial \bar{w}_0}{\partial x}\right) \quad \text{or} \quad M = \bar{M} \tag{28}$$

where Q is the shear force in the section obtained from the equilibrium of the differential element of the beam.

$$Q = \frac{\partial M}{\partial x} = B_{11}\frac{\partial^2 u_0}{\partial x^2} - D_{11}\frac{\partial^3 w_0}{\partial x^3} \tag{29}$$

2.4 Discretization by the Finite Element Method

2.4.1 Determination of the Stiffness Matrix

Herein, the classical beam element was chosen for treatment using FEM for formulation developed in the previous subsections [17]. This element is delimited by two nodes at its ends, with three degrees of freedom at each of these nodes: u_0, w_0, and $\frac{\partial w_0}{\partial x}$. The interpolation functions used to represent the displacements along the finite element of length L_{el} were cubic polynomials for $w_0 = w_0(x)$ and linear polynomials for $u_0 = u_0(x)$. Finally, the rotation $\frac{\partial w_0}{\partial x}$ was obtained by deriving from $w_0(x)$.

The FEM application generates a system of nodal equilibrium equations of type

$$[K]\{D\} = \{F\} \tag{30}$$

where $[K]$ is the global stiffness matrix of the structure, a function of both the geometry of the beam and the mechanical properties of the materials, and is given by the assembly of elements, as shown in Equation (31); $\{F\}$ is the global vector of loads, containing the equivalent nodal loads acting on the structure; and $\{D\}$ is the vector of nodal displacements, obtained by solving the system of Equations (30).

$$[K] = \sum_1^{NE} [k_{el}] \tag{31}$$

where NE is the number of finite elements defined in the beam discretization; and $[k_{el}]$ is the stiffness matrix of the beam element, which is given by

$$[k_{el}] = \begin{bmatrix} \frac{A_{11}}{L_{el}} & 0 & -\frac{B_{11}}{L_{el}} & -\frac{A_{11}}{L_{el}} & 0 & \frac{B_{11}}{L_{el}} \\ 0 & \frac{12D_{11}}{L_{el}^3} & \frac{6D_{11}}{L_{el}^2} & 0 & -\frac{12D_{11}}{L_{el}^3} & \frac{6D_{11}}{L_{el}^2} \\ -\frac{B_{11}}{L_{el}} & \frac{6D_{11}}{L_{el}^2} & \frac{4D_{11}}{L_{el}} & \frac{B_{11}}{L_{el}} & -\frac{6D_{11}}{L_{el}^2} & \frac{2D_{11}}{L_{el}} \\ -\frac{A_{11}}{L_{el}} & 0 & \frac{B_{11}}{L_{el}} & \frac{A_{11}}{L_{el}} & 0 & -\frac{B_{11}}{L_{el}} \\ 0 & -\frac{12D_{11}}{L_{el}^3} & -\frac{6D_{11}}{L_{el}^2} & 0 & \frac{12D_{11}}{L_{el}^3} & -\frac{6D_{11}}{L_{el}^2} \\ \frac{B_{11}}{L_{el}} & \frac{6D_{11}}{L_{el}^2} & \frac{2D_{11}}{L_{el}} & -\frac{B_{11}}{L_{el}} & -\frac{6D_{11}}{L_{el}^2} & \frac{4D_{11}}{L_{el}} \end{bmatrix} \tag{32}$$

During the process of applying loads on the structural element, the matrix $[k_{el}]$ can be different even for elements of the same length L_{el} because the cracking process of the concrete or the yielding of the reinforcement causes the damage variable to assume different values along the length or height of the beam.

2.4.2 Nonlinear Analysis

To reach the final equilibrium solution, incremental application of external loads was performed to obtain an initial (predicted) solution, followed by an iterative Newton–Raphson using force or displacement control process. Table 1 summarizes the flowchart of the program.

2.5 Model Validation

The experimental results obtained by Álvares [15] were used to validate the proposed model. Reinforced concrete beams with different reinforcement ratios were experimentally investigated to evaluate their failure form when subjected to a four-point bending test. The experimental test of the beams was performed with load control such that the test was interrupted when the breaking load was reached.

The beams evaluated by Álvares [15] had a rectangular section measuring 120 mm × 300 mm, with a span of 2400 mm and loads located 800 mm from the support, as shown in Figure 2a and 2b.

The reinforcement rate of the beams was varied such that three types of failures, namely flexural tension failure (under-reinforced section), flexural compression failure (over-reinforced section), and simultaneous failure (optimized section), could be evaluated. The upper reinforcement of all beams consisted of two bars with a diameter of 5 mm. The lower reinforcement varied based on the type of failure expected for the beam: i) for the under-reinforced section beam (Figure 2b), three bars with a diameter of 10 mm were used (A_s = 236 mm^2); ii) for the optimized section beam (Figure 2c), five bars with a diameter of 10 mm were used (A_s = 393 mm^2); iii) for the over-reinforced section beam (Figure 2d), seven bars with a diameter of 10 mm were used (A_s = 550 mm^2). For beam reinforcement, the following properties were assumed for steel: $E_s = 196$ GPa, $f_y = 500$ MPa, and $f_u = 500$ MPa.

For concrete modeling, an elastic modulus of 29.2 GPa and the following parameters necessary for the Mazar damage model, defined by Álvares [15], were used. $A_t = 995$, $B_t = 8000$, $A_c = 0.85$, $B_c = 1620$ and $\varepsilon_{d0} = 0.00007$. Additionally, a Poisson's ratio of 0.2 was assumed.

A convergence study (verification process) of the discretization parameters of the load–displacement solution was performed to determine the finite element mesh of the beams by varying the number of layers (10, 20, and 40 layers) of the cross section, the number of elements for the length of the beams (12, 24, 36, and 48 elements), the initial load step (0.5, 1.0, and 2.0 kN), and the tolerance of the iterative process (10^{-3}, 10^{-4}, and 10^{-6}). Therefore, the investigation recommended for the simulation of the three beams were a discretization of 20 layers and 36 elements, an initial load step of 1 kN and tolerance of 10^{-6}.

Table 1. Iterative process of obtaining a solution

Pre-cracking phase (D = 0)	Post-cracking phase (D > 0)
1. Calculation of the stiffness matrix; 2. The load is updated from the load increment $\{\Delta F\}$; 3. Solve the system of Equation (30); 4. Return to step 1;	1. Calculation of the stiffness matrix in relation to the last equilibrium configuration using displacements, strains, stresses, and the updated damage variable; 2. Update load from load increment $\{\Delta F\}$; 3. Solve the system of Equation (30); 4. Check convergence through the unbalanced force (external forces minus internal forces); 5. If there is no convergence, the stiffness of the structure must be updated and then the increment of the nodal displacements $\{\Delta D\}$must be calculated through the unbalance force. Subsequently, the displacements ($\{\Delta D\} + \{D\}$) and the damage variable are updated. Finally, the unbalanced force is updated and the convergence is verified (external force minus internal force). Repeat this process until the solution converges to that charge level. 6. After convergence, go back to step 1.

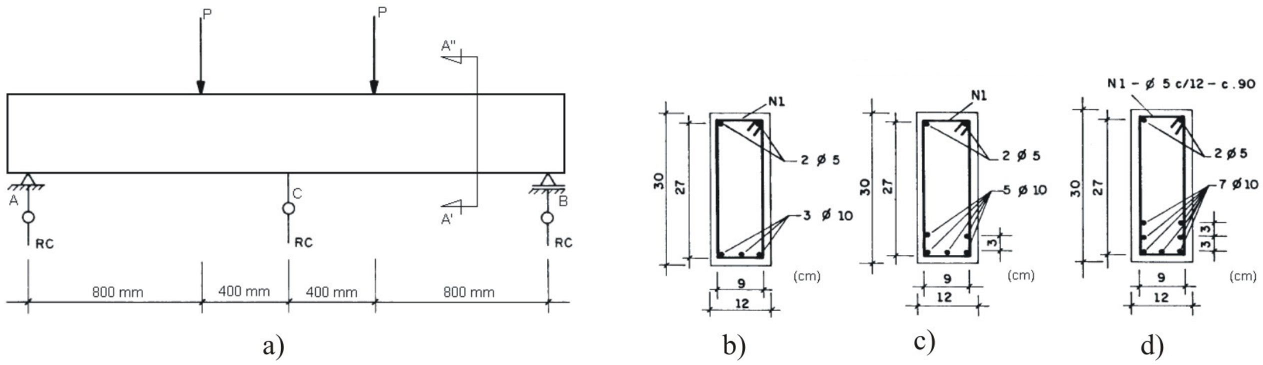

Figure 2. Experimental setup [15]: a) four-point bending test; b) under-reinforced beam; c) optimized beam; d) over-reinforced beam.

3. Results and Discussion

For the three types of beams, Figures 3~5 show the force–displacement curves obtained experimentally by Álvares [15] and the respective numerical results obtained from the proposed model. The experimentally acquired force–displacement curves exhibited the typical behavior of reinforced concrete beams subjected to bending failure, along with the identification of three stages (Figure 3). In Stage I, the concrete was undamaged, and the stiffness of the EI_I beams was because of the combined action of concrete and steel. The cracking of concrete indicates the end of this stage. The cracking load is defined by the tensile strength of the concrete.

In stage II, the curve initially exhibits nonlinear behavior that is characterized by the appearance of multiple cracks on the lower face of the beam. Gradually, stress is transferred to the steel bars, which provide the tensile strength of the beam. As the load increases, a second linear section is formed whose slope represents the stiffness EI_{II} of the cracked beam and is defined primarily by the reinforcement rate. However, the cracked concrete can contribute to the stiffness in a phenomenon called the tension-stiffening effect [18].

Stage III begins with a further reduction in the stiffness and a trend to stabilize the force until the beam fails. The reinforcement rate of the beam affects the force and displacements that define the beginning and end of stage III, which can lead to three types of failure associated with deformations in steel and concrete at the instant of beam collapse.

For stages I and II, a good approximation between the experimental load–displacement curves and the curves obtained using the proposed model, wherein the damage model is associated with the classical theory of laminates, can be confirmed by comparing the numerical results with the experimental results. However, the experimental curve presents an ultimate displacement during the beam test that is smaller than that predicted by the numerical result. This is because the load control used in the experiment halts the test when the maximum load is reached.

In the numerical model, taking the limits of deformation presented in Figure 6 as a reference, the beam failure was established by monitoring the strains in the most compressed concrete layer and in the most stressed steel layer. The ultimate limit states of a reinforced concrete beam can be established when the strain in the concrete reaches a value ε_{cu}= 0.35% because of compression failure, and/or by tensile failure when the strain in the steel reaches a value ε_{su}= 1.00% caused by crushing the compressed section. Balanced beams fail because of crushing of the compressed region; however, the strain in the steel is equal to or less than the yield strain ε_{sy}. When the beam cross-section and reinforcement ratio are optimally designed, failure occurs simultaneously in the top compressed layer and the most tensioned reinforcement section.

The proposed numerical model allows for the monitoring of the strains of the materials of the beam and the identification of the failure mechanism, as shown in Figure 7. In the over-reinforced beam, failure occurs by crushing the compressed region. This beam has the highest failure load, of the order of 73 kN, but a lower total displacement than the other beams analyzed. For the under-reinforced beam, the maximum load obtained was 81% lower than the load observed for the over-reinforced beam, and the deformation was 1.2 times greater. The optimized beam presents a load 46% less than the load observed for the over-reinforced beam, but with a deformation 1.3 times greater. In addition, this beam presents the best use of materials, which contributes to the reduction of energy consumption and non-renewable materials, thereby increasing the sustainability of the structures.

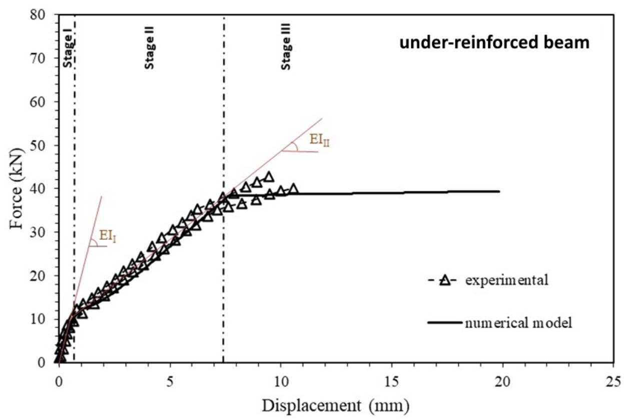

Figure 3. Flexural behavior of under-reinforced beam

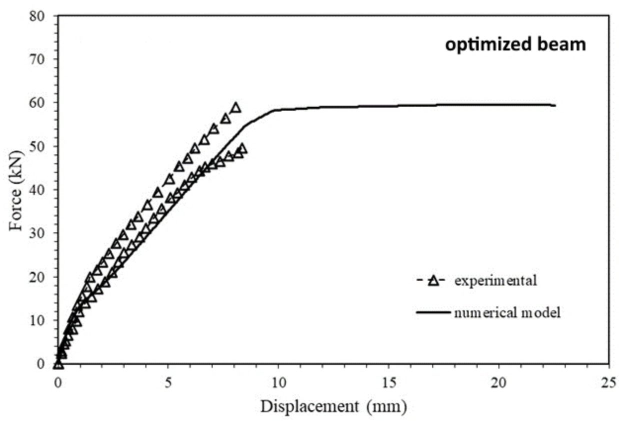

Figure 4. Flexural behavior of optimized beam

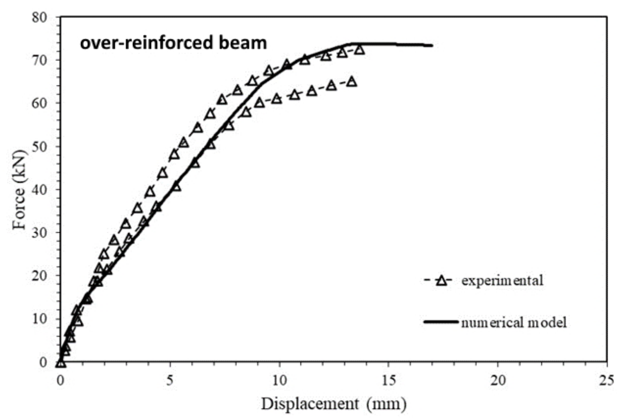

Figure 5. Flexural behavior of over-reinforced beam

The results obtained by the numerical model indicated a variation in the stress–strain behavior of each beam, as shown in Figure 8. For under-reinforced beams, the compressive stresses did not reach the peak stress but the stress–strain behavior was observed in the nonlinear regime at failure, thus indicating the appearance of damage to the stiffness of the concrete. As the strains in the reinforcement reached their maximum value, the neutral axis approached the upper surface of the beam section. For the other beams, the concrete had reached its ultimate strain, and the beam's neutral axis was close to the centroid of the cross-section.

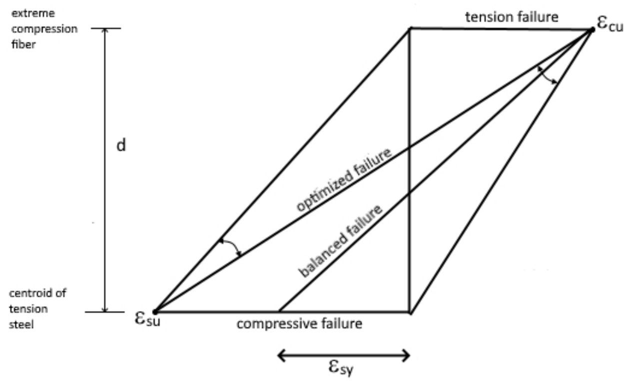

Figure 6. Strain limits for steel and concrete in the beam cross section

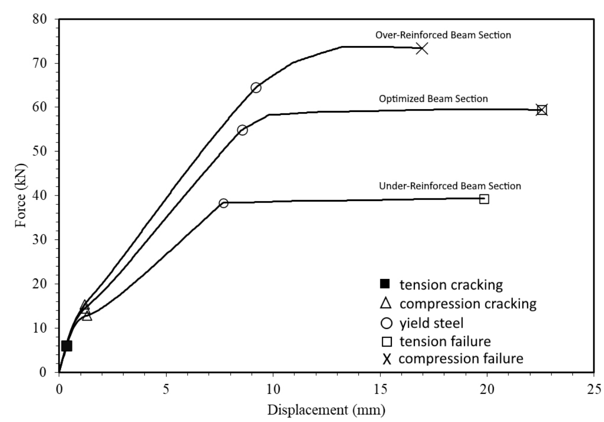

Figure 7. Theoretical identification of limiting strains of steel and concrete

Evidently, the proposed model for the behavior of tensioned concrete considers the contribution of cracking concrete (below the neutral axis), in contrast to design codes for reinforced concrete structures, even though the tensile stress value is low when comparing the stresses in the reinforcement and even in the compressed concrete.

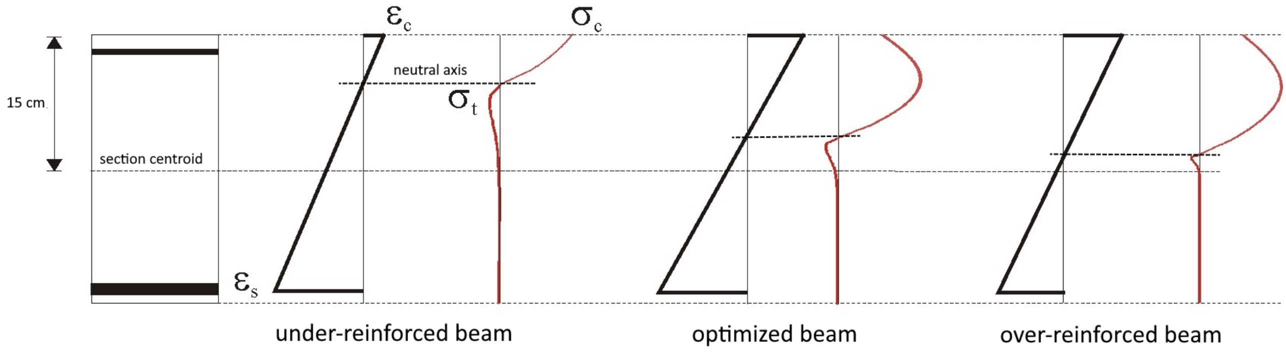

Figure 8. Stress–strain diagrams of concrete at failure of beam.

The variation in the stress–strain behavior is a function of the evolution of the damage parameter. As established by Equation (3), when the deformations exceed the limit value, ε_{d0}, there is a gradual reduction in the stiffness of the beam owing to cracking of the concrete. Figure 9 shows the variation in the damage parameter (1-D_c) for the three types of beams investigated, with the increase in the vertical displacement of the beam. Initially, the value of (1-D_c) was equal to unity because there was no damage to the compressed concrete. With increasing displacement, a reduction in this parameter was verified; however, it was affected by the reinforcement ratio of the beam. At failure, compression damage of approximately 60% was observed for under-reinforced beams, and the damage was approximately 80% for the optimized and over-reinforced beams.

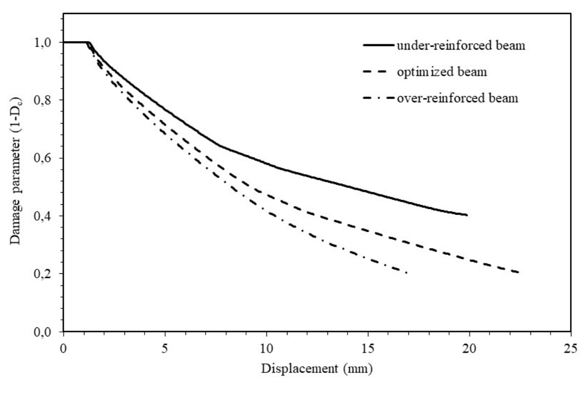

Figure 9. Variation in the damage parameter with increase in the vertical displacement of the beams.

4. Limitations of the Study

The model used in this study, within the scope of static loading, ignores shear and geometric nonlinearity effects. Furthermore, the Mazars damage model is elastic and is not appropriate for situations of cyclic loadings, which is not the case in the present study. However, the order of magnitude of the maximum transverse displacement of the beam with respect to the height is small, thus justifying the geometric linear analysis. The failure modes of the beams did not include shear failures.

5. Conclusions

The proposed model combines the classic theory of laminates and the Mazars damage model. By using FEM, it was able to evaluate the flexural behavior of reinforced concrete beams up to the failure of these elements for different rates of flexural using numerical simulation of the reinforced concrete beams under four-point bend tests. This was possible because the strategy of incorporating in the finite elements, the lamination of the transverse section, and the physical nonlinearity of the materials by continuous damage mechanics allowed the following of the stress and strain state of each layer of material, whether concrete (with its progressive cracking) or the reinforcement (even in the yielding).

Therefore, despite the relative simplicity of the proposed model, its potential to predict the behavior of reinforced concrete beams under bending was demonstrated, thereby allowing a precise identification of deformations and rupture criteria. The numerical model allowed the identification of the failure form of each type of reinforced concrete beam analyzed, through the prediction of the neutral line variation and the determination of the stress-strain behavior. In this way, the model can be used to predict the behavior of structural elements subjected to bending and lead to optimized designs, with greater safety and lower cost.

Author Contributions

JMFL: methodology, numerical modelling, formal analysis, writing - original draft; PRLL: conceptualization, investigation, data curation, formal analysis, writing - review & editing; GJBS: numerical modelling, formal analysis, writing - original draft.

Conflict of Interest

No conflict of interest.

Funding

This research was funded by CNPq, grant numbers 313693/2019-6 and 408135/2021-2, and State University of Feira de Santana, grant numbers 034/2021 and 064/2021.

References

[1] Wang, T., Hsu, T., 2001. Nonlinear finite element analysis of concrete structures using new constitutive models. Computer& Structures. 79, 2781-2791.

[2] Assan, A., 2002. Nonlinear analysis of reinforced concrete cylindrical shells. Computer&Structures. 80, 2177-2184.

[3] Tao, X., Phillips, D., 2005. A simplified isotropic damage model for concrete under bi-axial stress states. Cement & Concrete Composites. 27, 716-726.

[4] Mazars, J., Kotronis, P., Ragueneau, F., et al., 2006. Using multifiber beams to account for shear and torsion. Applications to concrete structural elements. Computer Methods in Applied Mechanics and Engineering. 195, 7264-7281.

[5] Butean, C., Heghes, B., 2020. Flexure Behavior of a two layer reinforced concrete beam. Procedia Manufacturing. 46, 110-115.

[6] Liu, C., Yang, Y., Wang, J., et al., 2020. Biaxial reinforced concrete constitutive models for implicit and explicit solvers with reduced mesh sensitivity. Engineering Structures. 219, 110880.

[7] Tjitradi, D., Eliatun, E., Taufik, S., 2017. 3D ANSYS numerical modeling of reinforced concrete beam behavior under different collapsed mechanisms. International Journal of Mechanics and Applications. 7(1), 14-23.

[8] Gorgogianni, A., Elias, J., Le, J.L., 2020. Mechanism-based energy regularization in computational modeling of quasibrittle fracture. Journal of Applied Mechanics. 87(9), 091003.

[9] Arruda, M.R.T., Pacheco, J., Castro, L.M.S., et al., 2022. A modified mazars damage model with energy regularization. Engineering Fracture Mechanics. 259, 108129.

[10] Carrera, E., Augello, R., Pagani, A., et al., 2021. Component-wise approach to reinforced concrete structures. Mechanics of Advanced Materials and Structures. 1-19.

[11] Arruda, M.R.T., Castro, L.M.S., 2021. Non-linear dynamic analysis of reinforced concrete structures with hybrid mixed stress finite elements. Advances Engineering Software. 153, 102965.

[12] Leone, F.A., Justusson, B.P., 2020. Effects of characteristic element length on fracture energy dissipation in continuum damage mechanics models. Journal of Composites Materials. 55(24), 3551-3566.

[13] Di Prisco, M., Mazars, J., 1996. Crush-crack': a non-local damage model for concrete. Mechanics of Cohesive-frictional Materials. An International Journal on Experiments, Modelling and Computation of Materials and Structures. 1(4), 321-347.
DOI: https://doi.org/10.1002/(SICI)1099-1484(199610)1:4<321::AID-CFM17>3.0.CO;2-2

[14] Mazars, J., Lemaitre, J., 1985. Application of Continuous Damage Mechanics to Strain and Fracture Behavior of Concrete. Shah, S.P. (eds) Application of Fracture Mechanics to Cementitious Composites. NATO ASI Series, vol 94. Springer, Dordrecht.
DOI: https://doi.org/10.1007/978-94-009-5121-1_17

[15] Alva, G.M.S., El Debs, A.L.H.C., Kaminski Jr, J., 2010. Nonlinear analysis of reinforced concrete structures in design procedures: application of lumped dissipation models. Revista IBRACON de Estruturas e Materiais. 3, 149-178.
DOI: https://doi.org/10.1590/S1983-41952010000200003

[16] Reddy, J.N., 2004. Mechanics of laminated composite plates and shells: theory and analysis. CRC Press. USA. pp. 831.

[17] Cook, R.D., Malkus, D.S., Plesha, M.E., et al., 2002. Concepts and applications of finite element analysis. John Wiley & Sons. Inc. USA. pp. 719.

[18] Martins, M.P., Rangel, C.S., Amario, M., et al., 2020. Modelling of tension stiffening effect in reinforced recycled concrete. Revista Ibracon de Estruturas e Materiais. 13, 1-21.